Dynamic model reference *PI* control of permanent magnet AC motor drives

Paul Stewart[a,*], Visakan Kadirkamanathan[b]

[a] *Department of Automatic Control and Systems Engineering, University of Sheffield. Mappin St. Sheffield, UK*
[b] *Department of Automatic Control and Systems Engineering, University of Sheffield. Mappin St. Sheffield, S1 3JD, UK*

Abstract

The permanent magnet AC motor drive (PMAC) is a multivariable, non-linear, closely coupled system subject to saturation due to finite DC supply voltage and hard current limits for protection of the drive hardware. Model following controls can be applied to this class of motor with *PI* current controllers enabling tracking of quadrature current command values. The presence of a finite supply voltage constraint results in reduced system performance when the current regulators saturate. A dynamic model reference controller is presented which includes the currents and voltage limits, constraining the magnitude of the command signals, operating the system to just within the bound of saturation, allowing the *PI* controllers to accurately track the commanded values and retain control of the current vectors. This regime ensures maximum possible dynamic performance of the system. The system and controller is simulated and experimentally verified, controller gain being found by Monte Carlo simulation.

Keywords: Saturation; Feedback linearisation; Model reference control; *PI* control

1. Introduction

The PMAC synchronous motor which is under consideration in this case study has three phase windings which are distributed to give a sinusoidal back EMF with the phase currents having a separation of 120° electrical. High performance rare earth permanent magnets are mounted on the surface of the rotor giving a "smooth rotor" device which does not exhibit any manifestations of saliency. A technique known as *d–q* analysis which has historically been applied to induction motors has been found to be an ideal tool both in terms of describing the machine, and designing control methods. The method has the advantages of simplicity, and an associated graphical description which facilitates understanding of the operating processes of the machine.

Applying the *d–q* transformation (Sudhoff, Corzine, & Hegner, 1995) transforms the three phase currents and voltages into an orthogonal reference frame rotating synchronously with the rotor flux. However a boundary exists known as base speed where the rising back EMF equals the supply voltage and no further torque production is possible (Jahns, Klimann, & Newmann, 1986). The speed range of the motor can be considerably extended beyond base speed by introducing negative *d* axis current, suppressing the *q* axis current. The object of the control action in this application will be to maximise the torque envelope developed by the motor above base speed both dynamically and in steady state. A secondary objective will be to minimise the magnitude of the current vector at all times in order to reduce i^2r losses in the motor. Traction drives and industrial spindle drives require the motor to operate in the constant power region shown in Fig. 1. The principal features of the operation are shown in this diagram; the constant torque region of operation where the applied voltage is larger than the back EMF, base speed which is the critical point where the applied voltage equals the back EMF voltage, and finally the constant power region where the back EMF voltage is larger than the applied voltage. The system can be described in the *d–q* reference frame by (Jahns, 1987)

$$V_q = ri_q + \omega L i_d + \omega\lambda + L\left(\frac{\mathrm{d}i_q}{\mathrm{d}t}\right), \tag{1}$$

*Corresponding author. Tel.: +44-0-114-2225670; fax: +44-0-114-2731729.

E-mail addresses: p.stewart@shef.ac.uk (P. Stewart), visakan@shef.ac.uk (V. Kadirkamanathan).

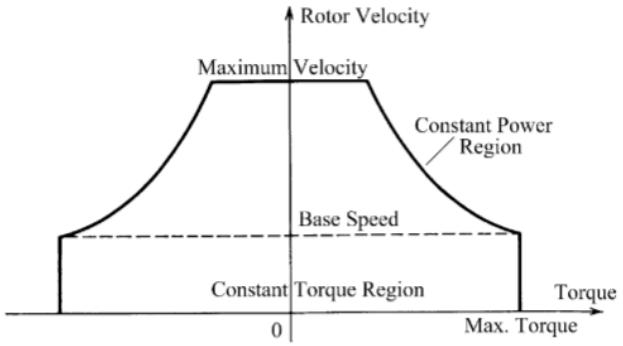

Fig. 1. Two quadrant torque–speed map illustrating base speed and constant power region.

$$V_d = ri_d - \omega L i_q + L\left(\frac{\mathrm{d}i_d}{\mathrm{d}t}\right), \tag{2}$$

$$T_e = k_t i_q, \tag{3}$$

where V_d and V_q are the d and q axis voltages, i_d and i_q are the d and q axis currents, r the phase resistance, λ the back emf constant, T_e the instantaneous torque output, L the phase inductance and k_t the torque constant. In this case with the non-salient rotor, $L_d = L_q = L$, so reluctance torque can be neglected. The motor operates subject to constraints on voltage and current

$$V^2 \geqslant V_q^2 + V_d^2, \quad I^2 \geqslant I_q^2 + I_d^2, \tag{4}$$

where V is the available DC voltage magnitude, and I the maximum current limit magnitude. Considering these constraints, maximum torque per amp operation can be achieved by controlling the d axis current to zero. The system layout in Fig. 2 shows the salient features of both the control and conversion features (signified by DSP) and the physical hardware of the motor and power electronics. It is proposed to utilise a model reference controller (Stewart & Kadirkamanathan, 1998) outputting d and q axis current commands which are tracked by PI current controllers as part of a feedback linearising controller. The two voltage commands are then converted to three applied phase voltages via the Park transform (Jahns, 1987) producing three phase currents in the PMAC. Position and velocity feedback from the motor is obtained from a 12 bit absolute position encoder, and a current regulated pulse width modulated (PWM) inverter is used to achieve the best approximation of sinusoidal current waveforms (Miller, 1993). The constant torque operation of the PMAC is not a novel subject area (Macminn & Jahns, 1991), (Pillay & Krishnan, 1989). Instantaneous torque control is achieved via current vector control in a transformed orthogonal reference frame. For the PMAC surface mount machine, the d axis current is controlled to zero to ensure maximum torque-per-amp operation. In order to extend the range of the machine beyond base speed, the performance degradation associated with current regulator saturation must be addressed allowing smooth transition into the constant power region. A series of developments based upon the onset of current errors evolved to enable the extended speed region via the injection of negative d axis current (Soong & Miller, 1994). The algorithms are extensions of basic feedforward control (Jahns, 1987; Dhaouadi & Mohan, 1990).

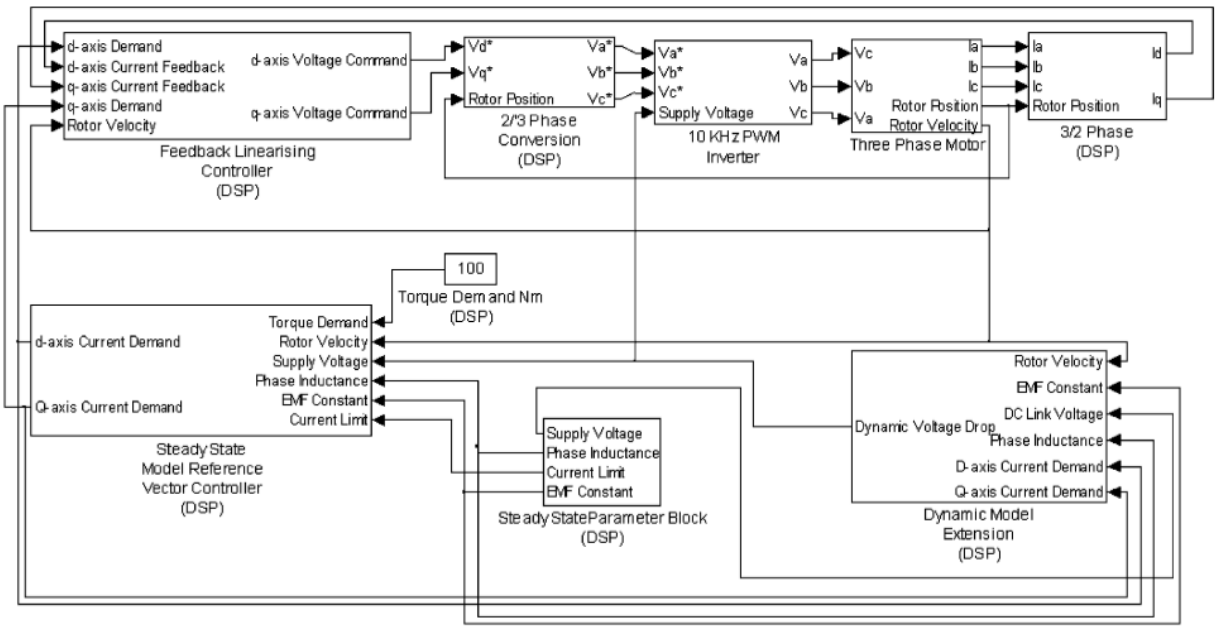

Fig. 2. Layout of motor and controller scheme.

Saturation of the current regulators is detected by increasing errors in the d axis current, which is very small in the constant power region due to high current regulator gains. The error detection serves to suppress the q axis current command, regaining at least partial control of the current vector. Steady-state experimental performance confirms the flux-weakening capability of this class of controllers. Since phase-advance is actuated by current controller saturation, insufficient voltage headroom exists to allow the current vector to *dynamically* follow the maximum torque envelope. A more sophisticated approach (Sudhoff et al., 1990; Morimoto & Takeda, 1994; Macminn & Jahns 1991; Chan, Jiang, Xia, & Chau, 1995) has been developed which unlike earlier methods does not rely upon current or voltage feedback from the motor to calculate the appropriate level of d and q axis current for flux weakening, relying instead on known machine parameters to perform the necessary calculations. The d and q axis current commands are derived either by real-time solution of the steady-state system equations, or by look-up table. These methods are shown to provide good performance in the flux-weakening region, and under steady-state conditions achieve the maximum torque-per-amp profile. Since the dynamic current components are neglected in the calculation of current commands, no voltage headroom is available to optimally advance the current vector under dynamic conditions. The subsequent degradation in current performance is particularly significant under dynamic no-load conditions such as gear-changing. In this paper, a dynamic model reference controller is presented, which reserves an appropriate amount of inverter voltage to allow the maximum torque envelope to be followed under dynamic conditions. State de-coupling is achieved by a non-linear feedback element, and losses reduced in the region below maximum torque by minimising the magnitude of the current vector at all times. For automotive drives applications, this results in maximum performance, and the shortest possible gear change times via an electronically actuated gearbox.

2. Model reference controller

A survey of the proposed flux weakening schemes in the literature demonstrate similar fundamental weakness. The key to the flux weakening control algorithms is to identify the onset of current regulator saturation, detection feedback being provided by the buildup of error between the commanded and actual d axis current. Fig. 3 is a simulation of the system freely accelerating under maximum torque command and no external inertial load and typical flux weakening controller as described in (Sudhoff et al., 1995). No information is given in any of the literature to calculate the gains for

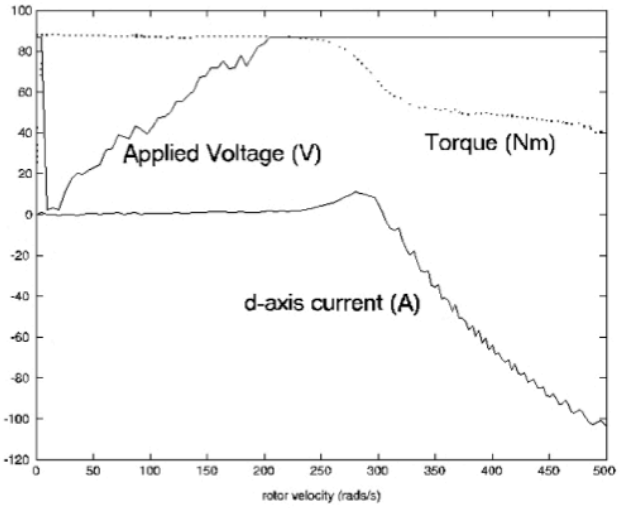

Fig. 3. Field weakening controller, dynamic operation, drive motor inertia only. Comparison of d axis current, supply voltage magnitude and produced torque.

any of the PID controllers present in the controllers to execute the automatic field weakening (Dhaouadi & Mohan, 1990). These controller gains are critical to supressing the q axis current demand and command negative d axis current. In order to perform this simulation, the gains were tuned "on the fly" to achieve the best possible torque speed envelope. It was found that the *PI* current regulators saturate (i.e. the voltage magnitude reaches a maximum) and torque production begins to tail off before any d axis current error is present. Error is detected by the existing methods when the d axis current goes positive. This flaw will result in a suboptimal torque-speed trajectory, its difference from the optimal path being a function of the system inertia. This simulation describes the worst case, since the motor is driving only its own rotor inertia, and the rate of change of current vector advance is at a maximum. In terms of actual operation, this reduced envelope can be ignored if ultimate performance is not the objective of the controller. The degradation will also be a function of how well the gains of the controller have been chosen and tuned. If the motor application specification requires the maximum torque speed profile to be the highest possible for the given DC link voltage and motor current limit, or it is necessary to perform servo operations on just the rotor inertia, then a controller must be developed which provides the maximum torque profile even in the low inertia servo case. In the case of the traction drive with a clutchless gearbox, the rotor velocity must be reduced by 50% and then track the output shaft velocity at minimum torque output to achieve gearchanging. This deceleration is a function of the maximum torque envelope and rotor inertia, and requires a controller to be designed which overcomes the

problem of accurately controlling the current vector in the face of *PI* current controller saturation. If we examine the applied voltage magnitude for the PMAC unconnected to any external load and accelerating freely under maximum torque demand as shown in Fig. 3, we can see that the applied voltage reaches the level of the DC link voltage (87 V) and the current regulators are saturated. It can be seen that any field weakening algorithm needs to be pre-emptive. The justification for this is that when the current regulators saturate, there is no voltage headroom available for dynamic control of the current vector and consequently optimal current control is lost. The effect of this saturation is most graphically shown in Dhaouadi and Mohan (1990), which confirms the results of the simulation shown in Fig. 3. Again the supply voltage is shown to saturate, and although torque production continues into the field weakening region, errors develop between the actual and commanded d and q axis currents which are eventually resolved, but the torque envelope is much reduced. The approach used in the design of the model reference controller will be to allow the current vector to follow its optimal path by including the non-linear saturation effects in the model.

3. Modes of control

The operating principle of model reference control systems is to specify system performance, using a model which gives the desired output for a given input. The form of the model can be hardware (for example the output of an op-amp.) or software (a mathematical model of the plant.). The controller compares the output of the model with that of the plant, and the control signals are generated as a function of the difference between plant and model. Thus, in the case of the PMAC motor, a model reference will be derived from the analytic solution of the system equation under the constraint of minimum current vector magnitude at all times. The output of the model provides reference values for the d–q components of the current vector. Rearranging the system equations (1) and (2) and neglecting resistance gives the reference model

$$i_q^* = V_q^* - \omega L i_d^* - \omega\lambda, \tag{5}$$

and by substituting Eqs. (4) into the supply voltage constrained voltage vector

$$V = \sqrt{V_q^{*2} + V_d^{*2}}, \tag{6}$$

and the expression for instantaneous torque

$$T_e^* = \frac{3P}{2}\phi_f i_q^* = k_t i_q^*, \tag{7}$$

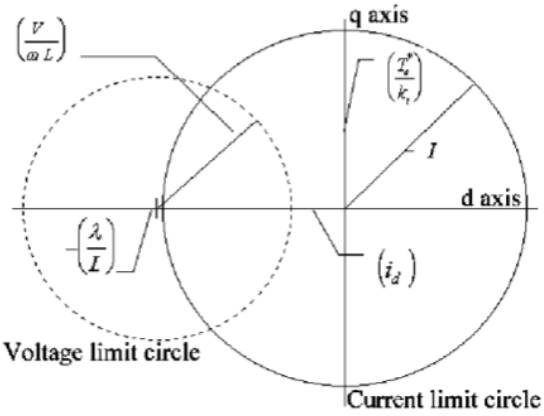

Fig. 4. Dimensions of the circle diagram description in terms of the system parameters.

yields an expression which describes the torque producing component of the system in terms of the physical parameters, torque constant k_t and speed variable ω;

$$T_e^* = \frac{k_t}{\omega L}\sqrt{V^2 - \omega^2\lambda^2} \tag{8}$$

$$= k_t\sqrt{\left(\frac{V}{\omega L}\right)^2 - \left(\frac{\lambda}{L}\right)^2} \tag{9}$$

also

$$V^2 = (\omega L i_d^* + \omega\lambda)^2 - (\omega L i_q^*)^2. \tag{10}$$

Combining Eqs. (9) and (10) yields

$$\left(\frac{V}{\omega L}\right)^2 = \left(i_d^{*2} + \frac{\lambda}{L}\right)^2 + \left(\frac{T_e^*}{k_t}\right)^2, \tag{11}$$

which describes the frequency dependent voltage vector in terms of the current components. This is graphically shown (Fig. 4) and forms the model for calculating the system command outputs for the three PMAC drive operating modes.

3.1. Model reference controller: operating mode 1

Operating mode 1 is defined when the motor is operating below base speed, and the requested torque is available, that is

$$\left(\frac{V}{\omega L}\right)^2 \geqslant \left(\frac{\lambda}{L}\right)^2 + \left(\frac{T_e^*}{k_t}\right)^2 \tag{12}$$

Therefore the solution for the torque component i_q is $I \geqslant i_q^*$. In this mode, the requested torque is available up to the rotor frequency

$$\omega = \frac{V}{L\sqrt{(\lambda/L)^2 + (T_{emax}^*/k_t)^2}}. \tag{13}$$

Since the current vector lies completely within the voltage circle, then $i_d^* = 0$, and $T_{emax}^* = k_t I$.

3.2. Model reference controller: operating mode 2

In operating mode 2, the demanded torque is available, however the injection of negative d axis current is required. Operating under the constraint of minimising the current vector,

$$min\,|i_d^*| = \left(\frac{\lambda}{L}\right) - \sqrt{\left(\frac{V}{\omega L}\right)^2 - \left(\frac{T_e^*}{k_t}\right)^2}, \tag{14}$$

the maximum torque available at any given rotor velocity in the flux weakening region can be derived. Since

$$I^2 = \left(\frac{T_e^*}{k_t}\right)^2 + i_d^{*2} \tag{15}$$

and

$$\left(\frac{V}{\omega L}\right)^2 = \left(\frac{T_e^*}{k_t}\right)^2 + \left(\frac{\lambda}{L} - i_d^*\right)^2, \tag{16}$$

solving for T_e^* based on Eq. (15) gives

$$\left(\frac{T_e^*}{k_t}\right)^2 = I^2 - i_d^{*2} \tag{17}$$

and based on Eq. (16) gives

$$\left(\frac{T_e^*}{k_t}\right)^2 = \left(\frac{V}{\omega L}\right)^2 - \left(\frac{\lambda}{L} - i_d^*\right)^2. \tag{18}$$

It is possible to find the value of i_d^* corresponding to maximum torque demand at any velocity in the field weakening region, and also to calculate the maximum torque available at that velocity. The current i_d^* is solved to give

$$sin\,\theta = \frac{T_{emax}^*}{k_t I_{smax}} \tag{19}$$

and

$$cos\,\theta = \frac{i_d^*}{I_{smax}}, \tag{20}$$

where θ is the advance angle of the current vector.

3.3. Model reference controller: operating mode 3

In this mode of operation, the requested torque is not available at a particular operating frequency. The controller should now ideally output the maximum torque which *is* available. Maximum available torque corresponds with the intersection of the current and voltage circles which correspond to the hardware current limit for device protection and available DC link voltage, respectively. This is described as follows:

$$\sqrt{\left(\frac{\lambda}{L}\right)^2 + \left(\frac{T_e^*}{k_t}\right)} \geqslant \left(\frac{V}{\omega L}\right)$$

$$\geqslant \left(\sqrt{I^2 - \left(\frac{T_e^*}{k_t}\right)^2} + i_0\right)^2 + \left(\frac{T_e^*}{k_t}\right)^2, \tag{21}$$

where i_o is λ/L. The logical operation of the model reference controller is given in Fig. 5.

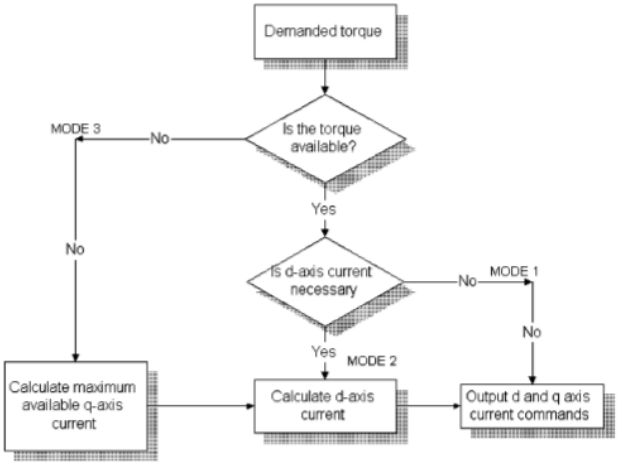

Fig. 5. Model reference controller decision tree.

3.4. Dynamic extension

Expressions have previously been derived (Stewart & Kadirkamanathan, 1999) to describe both the voltage drop due to dynamic effects of the advancing current vector in the flux weakening region, which is given as

$$V_{drop} = \sqrt{\left(L\frac{di_d}{dt}\right)^2 + \left(L\frac{di_q}{dt}\right)^2}, \tag{22}$$

and also the new base speed associated with this dynamic effect which is given as a solution for ω of

$$0 = -\sqrt{I^2 + \frac{\lambda^2}{L^2}}\omega^2 L + V_s\omega \tag{23}$$

$$- \frac{ILk_t(L^2I^2 + \lambda^2)}{\lambda J}. \tag{24}$$

The requirements of the flux weakening controller are to calculate the rotor velocity at which flux-weakening is to be initiated, and to output optimal d and q axis current commands in steady-state and dynamic operation. The most convenient description of the system is the steady state circle diagram, in the d–q reference frame. Now in the steady-state model reference controller, the current vector I is calculated as extending from $(0, 0)$ in the d–q frame to the intersection of the current limit circle and

the frequency related voltage limit circle with radius $V/\omega L$ and centre $(-\lambda/L, 0)$ as shown in Fig. 6. The outputs of the model reference are the command quantities i_q^* and i_d^* based on the geometrical representation shown in Fig. 6. In order to reserve sufficient voltage headroom to allow the current dynamics to act effectively, the length of the frequency related voltage limit vector $V/\omega L$ must be reduced by an appropriate amount. The voltage reserved for this effect has d and q axis components and can be described as being a vector extending from the voltage limit vector in the model reference as shown in Fig. 7. The d and q axis current commands are now formulated as the intersection of the dynamic voltage drop (which augments the steady state voltage limit vector) and the current limit circle. For the benefit of reduced computation in the model reference controller, the voltage drop due to the dynamics can be approximated as a worst case. That is the magnitude of the dynamic voltage drop is calculated and subtracted from the magnitude of the voltage limit vector, the new voltage limit vector including the dynamic components being represented as V_{lim}.

$$V_{lim} = \frac{\lambda}{\omega L} - \left(\sqrt{\left(L\frac{\mathrm{d}i_d}{\mathrm{d}t} \right)^2 + \left(L\frac{\mathrm{d}i_q}{\mathrm{d}t} \right)^2} \right). \tag{25}$$

Similarly, the unmodelled voltage drop due to resistive effects can be included as a worst case effect, and thus the voltage limit vector now contains all the significant system voltage drops, with any minor unmodelled drops being lumped together in the worst case adoption of vector directions. The voltage limit vector now becomes

$$V_{lim} = \frac{\lambda}{\omega L} - \left(\sqrt{\left(L\frac{\mathrm{d}i_d}{\mathrm{d}t} \right)^2 + \left(L\frac{\mathrm{d}i_q}{\mathrm{d}t} \right)^2} \right) - \left(\sqrt{(ri_q)^2 + (ri_d)^2} \right). \tag{26}$$

If this voltage can be reserved in operation, coupled with a revised base speed to enable the reservation process, then the machine should follow the optimal current trajectory with current regulators held within the bounds of saturation. The geometric implementation in the model reference controller is shown in Fig. 8. The calculations involved in the implementation of this algorithm are relatively straightforward. In steady state form, the reference model is supplied by a set of memory registers which contain the parameters neccessary to calculate the circle diagram representation with voltage and current limit vectors. The value for DC link supply voltage is measured directly from the DC supply which is either a battery or Ward–Leonard DC generator. The reserved voltage headroom calculated by utilising Eq. (22) to calculate the magnitude of the dynamic voltage drop, and adding to it the resistive part of Eq. (26). This value can now be subtracted from the

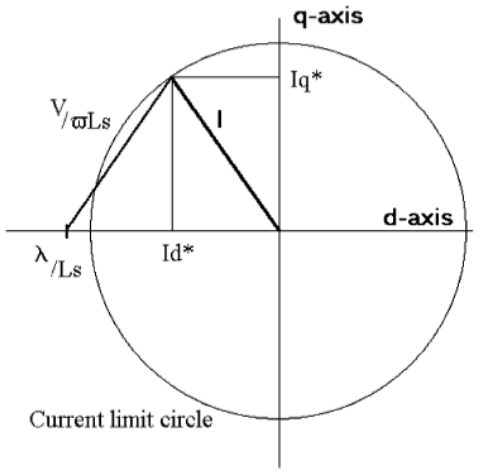

Fig. 6. PMAC motor as described by the steady-state model reference implementation.

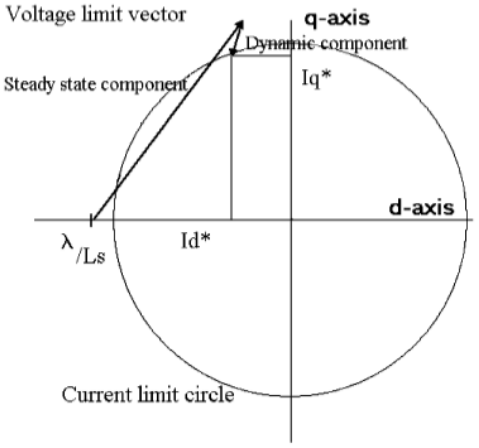

Fig. 7. PMAC motor as described by the steady-state model reference implementation, augmented by dynamic voltage drop vector.

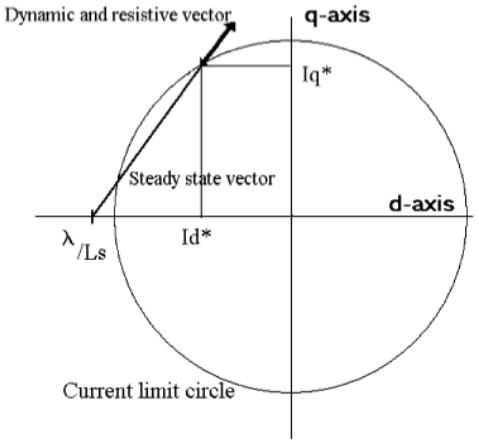

Fig. 8. PMAC dynamic model reference control geometric implementation.

measured DC link value, the new value being supplied to the steady-state model reference controller. This revised DC link value is appropriate to the steady-state description, with the correct value of voltage reserved to allow dynamic operation, and the unmodelled resistive voltage drop now included. The model reference outputs command values as before and is unaware that voltage has been reserved for dynamic operation. The final part of the implementation is the calculation and use of the revised base speed. An expression has been derived to calculate the new dynamic base speed in Eq. (24). This value is used to switch the voltage reservation algorithm in and out. Below dynamic base speed, the dynamic voltage drop is not subtracted, subtraction only taking place above this new dynamic base speed.

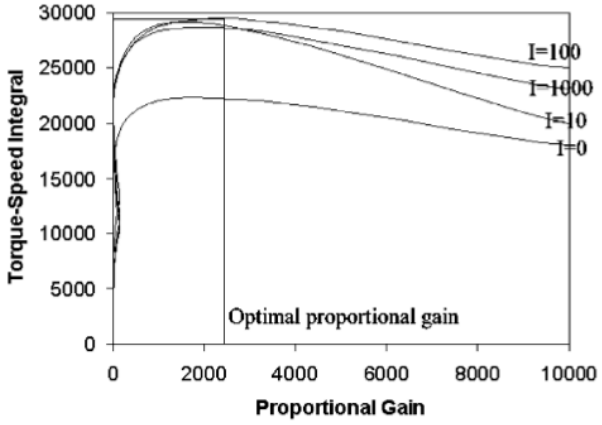

Fig. 9. Examples of integral gain performance profiles graphed against proportional gain.

4. *PI* feedback linearising controller

The PMAC motor equations are cross-coupled and bilinear in its states. Non-linear feedback elements must therefore be designed (Hunt, 1983) such that accurate current tracking is achieved. The feedback linearisation schemes described in the literature (e.g Morimoto & Takeda, 1994) are based upon steady-state descriptions of the system. In order to decouple and linearise the system for dynamic operation, the existing method has been extended to include the dynamic current errors. The feedback linearising control law is given by

$$V_d = ri_d - \omega L i_q + V_1 L, \tag{27}$$

$$V_q = ri_q + \omega(Li_d + \lambda) + V_2 L, \tag{28}$$

where the auxilliary inputs are designed as

$$V_1 = \frac{\mathrm{d}i_d^*}{\mathrm{d}t} + ki_d^* - ki_d, \tag{29}$$

$$V_1 = \frac{di_q^*}{\mathrm{d}t} + ki_q^* - ki_q. \tag{30}$$

Decoupling of the current loops is achieved, resulting in improved current regulator control, and consequently accurate tracking of the model reference command trajectories. This results in error dynamics of

$$\frac{\mathrm{d}\underline{e}}{\mathrm{d}t} + k\underline{e} = 0, \tag{31}$$

where

$$\underline{e} = \begin{vmatrix} i_d^* - i_d \\ i_q^* - i_q \end{vmatrix}. \tag{32}$$

No rigorous tuning scheme exists to tune the *PI* gains for the *d* and *q* axis current controllers since the system is multivariable and non linear and therefore outside the scope of, for example Ziegler–Nichols tuning method for SISO systems (Zhuang & Atherton, 1993). In practice, the gains are usually tuned on the fly experimentally slowly increasing the proportional gains to achieve good dynamic performance, and then increasing the integral gains to remove any steady-state errors that exist. Due to the sharp rise in computational power in even the domestic PC, it has become possible to apply a Monte Carlo analysis of the system to perform a global search to find the optimal gains for dynamic performance. The algorithm searches all combinations of controller gains within bounded values of 0–10000 for the proportional gain and 0–1000 for the integral gain. A differential term is not included in the controllers due to the presence of current measurement noise. It was initially ascertained through a set of simulations at random gain values that the gain values chosen must be equal in the *d* and *q* axis controllers to provide a balanced control action. A simulation was run with the dynamic controller commanding full acceleration for a rotor only inertia from 0 to 400 rad s^{-1} for every combination of gains within the search space for a step size of 10. Each simulation produced a waveform of rotor velocity versus torque, and in order to assess performance, each waveform was integrated with respect to velocity to find the *PI* combination which produces the maximum possible torque speed profile. The waveforms shown in Fig. 9 are a sample of typical output waveforms. The algorithm written in Matlab produces a waveform for each integral gain value versus the entire range of proportional gain values. For each waveform, the maximum value is found, for example in the diagram an optimal proportional gain is found for an integral gain of 100. These results are then correlated to find the optimal *PI* pair, which was found to be $P = 2000$ and $I = 110$. These are the values which were used for the subsequent experimental verification, and correlated closely with the gain values found experimentally (Fig. 9).

5. Experimental results

The algorithms proposed were implemented on an experimental dynamometer test rig. In each case the rotor accelerates freely from rest under a controller which is seeing a maximum torque demand. The controller is tested on both a rotor alone, and also when the motor is connected to the external load motor. The torque speed profile is not directly measurable, and is derived from the q axis current calculated by the $3-2$ transform on the DSP, outputted to a computer via the D/A port, and converted to a torque value via the torque constant k_t. The torque constant as given by the motor producer is defined for a motor at room temperature. In order to maintain the accuracy of the calculation, all profiles presented here were performed on a motor which had returned to ambient temperature after its last test (as measured by in built thermocouples). Fig. 10 presents the torque profiles of the dynamic and steady-state controllers operating dynamically and driving the external load motor. Simulations predicted waveforms which correlate closely with the experimental waveforms. The torque profile of the steady-state controller declines more rapidly at base speed than would be expected, which can be justified by the unmodelled voltage drop and parameter errors. The dynamic controller shows itself to be robust and correlates closely with the predicted profile. Since the current regulators are held on the operational side of the saturation limit, unmodelled effects or parameter errors are catered for by the reserved voltage. When the load motor is disconnected and the experiment repeated, the simulated prediction of performance is again confirmed and is presented in Fig. 11. The maximum achievable torque profile has been calculated from the system equations. As in the experiment driving the external load, the steady-state performance drop is more severe

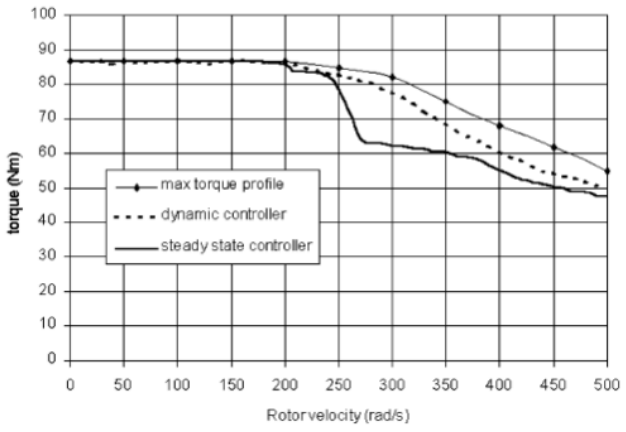

Fig. 10. Experimental torque profiles of the steady state and dynamic controllers, compared to the maximum achievable torque profile, connected to external load.

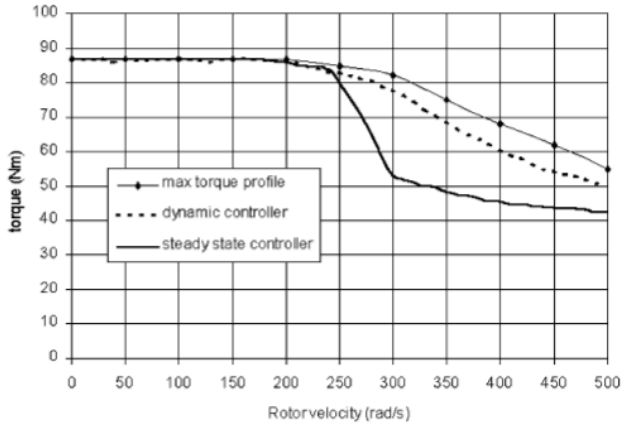

Fig. 11. Experimental torque profiles of the steady state and dynamic controllers, compared to the maximum achievable torque profile, rotor only load.

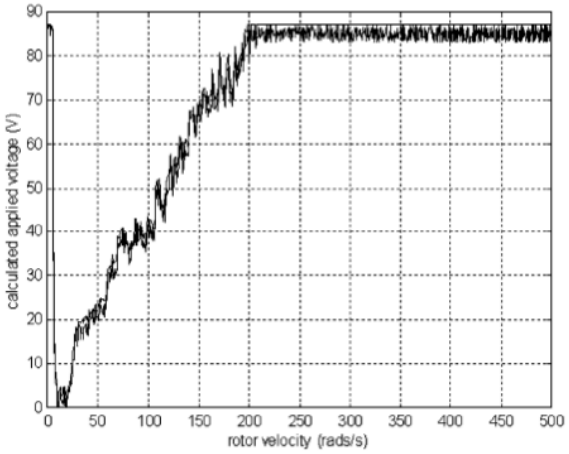

Fig. 12. Applied voltage magnitude, experimental comparison of dynamic and steady state controller.

than that predicted in simulation, again the dynamic controller correlates closely with its predicted behaviour. The magnitude of the applied voltage can be measured directly from the DSP board outputting the PWM signals to the inverter. The PWM synthesiser is supplied with modulation depth commands which are translated into three phase PWM signals. The magnitude of the applied voltage can therefore be calculated from the measurement of DC link voltage and the depth of modulation. Examination of Fig. 12 reveals the predicted action of the dynamic and steady state controllers. At the boundary with the field weakening region, the steady state current controllers saturate, and the applied voltage is subject to a PWM modulation depth of 100%. The dynamic controller operates just within the saturation limit, and thus maintains control of the current vector at all times throughout the operating range of the motor.

6. Conclusion

A model reference controller has been designed with a non-linear representation including the constraints of the system. Without the inclusion of these constraints, the *PI* regulators saturate and current control is lost. The constraints when applied to the model reference controller allow the *PI* current regulators to accurately track the model reference command values, and achieve an optimal torque speed trajectory.

Appendix. Motor parameters

Parameter	Value
L	0.000102 H
R	0.022 Ω
k_e	0.23 V/rad/s
V_{max}	87 V
I_{max}	200 A(rms)
T_{emax}	87 Nm

References

Chan, C. C., Jiang, J. Z., Xia, W., & Chau, K. T. (1995). Novel wide range speed control of permanent magnet brushless motor drives. *IEEE Transactions on Power Electronics*, *10*(5), 539–546.

Dhaouadi, R., & Mohan, N. (1990). Analysis of current regulated voltage-source inverters for permanent magnet synchronous motor drives in normal and extended speed ranges. *IEEE Transactions on Industry Applications*, *5*(1), 137–144.

Hunt, R. (1983). Design for multi input non linear systems. Differential geometric control theory (pp. 268–298). New York: Burkhauser.

Jahns, T. M., Kliman, G. B., & Neumann, T. W. (1986). Interior permanent magnet synchronous motors for adjustable speed drives. *IEEE Transactions on Industry Applications*, *IA-22*, 738–747.

Jahns, T. M. (1987). Flux-weakening regime operation of an interior permanent-magnet synchronous motor drive. *IEEE Transactions on Industry Applications*, *IA-23*, 681–689.

Macminn, S. R., & Jahns, T. M. (1991). Control techniques for improved high-speed performance of interior PM synchronous motor drives. *IEEE Transactions on Industry Applications*, *IA-27*, 997–1004.

Miller, T. J. E. (1993). *Brushless permanent magnet and reluctance motor drives*. Oxford, UK: University Press.

Morimoto, S., & Takeda, Y. (1994). Wide speed operation of interior permanent magnet synchronous motors with high performance current regulator. *IEEE Transactions on Industry Applications*, *30*(4), 920–926.

Pillay, P., & Krishnan, R. (1989). Modeling, simulation, and analysis of permanent magnet motor drives. Part I: The permanent-magnet synchronous motor drive. *IEEE Transactions on Industry Applications*, *IA-25*, 265–273.

Soong, W. L., & Miller, T. J. (1994). Field-weakening performance of brushless synchronous AC motor drives. *IEE Proceedings B-Electrical Power Applications*, *141*(6), 331–339.

Stewart, P., & Kadirkamanathan, V. (1998). On steady state and dynamic performance of model reference control for a permanent magnet synchronous motor. *UKACC International conference on control '98*, *Swansea*, *U.K.* (455) 664–669.

Stewart, P., & Kadirkamanathan, V. (1999). Dynamic control of permanent magnet synchronous motors in automotive drive applications. *1999 American control conference* (pp. 1677–1681). San Diego, USA.

Sudhoff, S. D., Corzine, K. A., & Hegner, H. J. (1995). A flux-weakening strategy for current regulated surface mounted permanent magnet machine drives. *IEEE Transactions on Energy Conversion*, *10*(3), 431–437.

Zhuang, M., & Atherton, D.P. (1993). Tuning of optimum PID controllers. *Proceedings of the IEE*, (140) 216–224.